Applied Chemical Engineering (2026) Volume 9 Issue 4 ISSN: 2578-2010 (O)
doi: 10.59429/ace.v9i4.6030

RESEARCH ARTICLE

Synthesis, Characterization, Molecular Docking, and Antibacterial Activity of a Novel Pyridine-Based Schiff Base and Its Copper(II), Silver(I), and Gold(III) Complexes

Ali Maki Kamel, Widad Ibrahem Yahya*

Department of Chemistry, College of Science, University of Kufa, Najaf, Iraq

***Corresponding author:** Widad Ibrahem Yahya, widadi.atyah@uokufa.edu.iq

ABSTRACT

Cu(II), Ag(I), and Au(III) complexes were synthesized from a new organic Schiff base ligand (PMBD),4-(pyridin-3-ylimino)methyl) benzene-1,3-diol, derived from a pyridine heterocycle, and 2,4-dihydroxybenzaldehyde. Spectroscopy techniques, XRD, and SEM data confirmed that the ligand acts as a bidentate mono-deprotonated coordinator, yielding nanoparticle-sized complexes with octahedral, tetrahedral, and square planar structures, respectively. The antibacterial activity in vitro against Escherichia coli and Staphylococcus aureus using the agar well diffusion method, minimum inhibitory concentration (MIC), and minimum microbicidal concentration (MMC) tests was supported by computational work simulating molecular docking against DNA gyrase units (1KZN and 2XCS). The experimental results showed that synthesizing the metal complexes significantly enhanced antibacterial activity compared to the free Schiff base ligand. The Cu(II) complex showed the strongest activity, with the largest inhibition zones measuring 37 mm, followed by the Ag(I) complex (26 mm), and finally the Au(III) complex (14 mm). Computational molecular docking binding studies indicate that the [Cu(L)2(H2O)2] Complex has the highest affinity against E. coli (1KZN) with a binding score of -7.3 kcal/mol and the lowest Ki value (4.42 µM) compared to the free Schiff base ligand (Ki = 12.21 µM). Conversely, the [Au(L)Cl2] complex displayed a lower binding energy of (-5.4 kcal/mol) and a higher Ki (109.43 µM) against 2XCS, aligned with its reduced experimental potency. The synthesized Schiff base ligand and its metal complexes demonstrate promising in vitro and in silico antibacterial activities via potential DNA gyrase inhibition. These findings suggest their high potential for further development in pharmaceutical and industrial antimicrobial applications.

Keywords: Metal complexes, DNA gyrase, Coordination chemistry, antimicrobial agents, Molecular Docking.

ARTICLE INFO

Received: 18 May 2026
Accepted: 28 September 2026
Available online: 04 November 2026

COPYRIGHT

Copyright © 2026 by author(s).
Applied Chemical Engineering is published by Arts and Science Press Pte. Ltd. This work is licensed under the Creative Commons Attribution-NonCommercial 4.0 International License (CC BY 4.0).
https://creativecommons.org/licenses/by/4.0/

Contribution/ Originality

This study contributes in the existing literature by synthesizing and characterizing a novel pyridine-based Schiff base ligand and its nano-sized Cu(II), Ag(I), and Au(III) complexes. It is one of the very few studies that have investigated comparative in silico docking validation against DNA gyrase coupled with in vitro antibacterial benchmarking, proving that metal complexation significantly enhances microbial eradication.



Graphical Abstract

1. Introduction

Aminopyridine ligands have been extensively studied in the synthesis, structure, and characterization of many coordination metal compounds. Schiff bases are condensation products of primary (aromatic) amines with aldehydes carrying the azomethine (imino) moiety (-CR=N-). They are considered versatile pharmacophores for various pharmacological activities, in which the azomethine group is critical to bioactivity. For example, Schiff bases, whether of natural or non-natural origin, have exhibited promising activity against various pathogens, including antibacterial, antitubercular, antifungal, antiparasitic, antiviral, antioxidant, and anticancer effects [1–3]. Schiff bases exhibit a broad spectrum of well-known biological effects. The rapid progress in pharmaceutical and medicinal chemistry has drawn scientists' attention to the development of drugs [4,5]. This study focuses on developing antibacterial compounds to overcome drug resistance and reduce the difficulties associated with the side effects of current medications. For this purpose, the Schiff base 4-((pyridin-3-ylimino)methyl)benzene-1,3-diol and its Cu(II), Ag(I), and Au(III) metal complexes have been synthesized. The ligand and its metal complexes were analyzed using Fourier Transform Infrared (FTIR), Proton Nuclear Magnetic Resonance (^{1}H NMR), Mass Spectrometry, and X-ray Diffraction (XRD). The antibacterial activity was tested against both Gram-positive bacteria (*Staphylococcus aureus*) and Gram-negative bacteria (*Escherichia coli*). The ligand and its metal complexes exhibited significant antibacterial activity against the tested strains. Additionally, the second section includes a comprehensive review of relevant literature and previous studies. The subsequent section also includes the data and methodology, including the experimental setup, characterization techniques, and computational docking protocols. The fourth section presents the results and detailed discussions for both the characterization and biological assays. Finally, the study concludes by comparing the synthesized compounds with standard drugs, where the main goal of the study is to produce compounds that require fewer steps in the process to generate a large quantity and have slightly better antibacterial activity than standard drugs, concluding with recommendations for future work.

2. Literature Review

Resistant bacterial strains have significantly reduced the effectiveness of traditional antibiotics, creating a growing need for new drugs. Schiff bases derived from pyridine and their complexes have emerged as key as major candidates in inorganic chemistry due to their diverse coordination structures and increased bioavailability. Many previous studies have varied, and a lot of them have shown that different Schiff base compounds have antimicrobial properties. However, most studies were limited to standard lab tests, without really diving into theoretical enzyme pathways, like how they inhibit DNA gyrase topoisomerase enzymes. Even though Cu (II) and Ag (I) compounds are very common, it's rare to find studies that directly compare them to Au (III) structures at the nanoscale. This study clearly addressed this gap by combining nanotechnology with molecular docking, supported by computational and laboratory evaluation. Recently, In 2025[6], A. Z. El-Sonbati et al. synthesized a Schiff base ligand derived from pyridine with its Cu(II), Co(II), Ni(II), Mn(II), and UO_2(II) complexes. Its structure was confirmed through spectral analyses, and biological tests showed it has more noticeable antifungal activity than antibacterial activity. However, El-Sanabati and his colleagues focused on large-sized formations with antifungal results that can be compared with our current study, where we took a different research approach. We systematically move to the nanoscale to improve bacterial membrane penetration and increase antibacterial efficacy. In addition, our work provides a new computer-based comparison that strictly focuses on bacterial DNA nuclease units (1KZN and 2XCS) using trivalent gold structures along with divalent copper and monovalent silver complexes, successfully bridging the gap between nano-synthesis and biological inhibition.

In 2025, another related study by Putri Dwi Lestari [7] examined the single-crystal X-ray diffraction (SC-XRD) of a nickel (II) complex, which showed the distorted octahedral shape derived from aminopyridine. While their structural investigation provided high crystallographic analyses, the biological evaluation yielded

relatively low antibacterial efficacy against *Staphylococcus aureus* and *Escherichia coli*, with a maximum inhibition zone of only 6.90 mm, attributed to a mild synergistic membrane disruption. In comparison to Lestari's work, our current investigation offers distinct evolutionary advantages in both synthetic efficiency and biological potency. Rather than relying on prolonged crystallization timeframes (such as 35 days), we implemented a streamlined synthetic protocol yielding tailored nano-sized architectures confirmed via SEM and XRD. This drastic reduction into nanoscale dimensions exponentially amplified the antibacterial performance, as evidenced by our Cu(II) complex achieving an inhibition zone of 37 mm, which is remarkably superior to the 6.90 mm reported by Lestari. Furthermore, while their study focused on internal crystal packing interactions, our research transcends structural confinement to validate the real-world therapeutic potential through targeted in silico molecular docking profiling against DNA gyrase subunits, successfully elucidating the precise mechanism behind the enhanced bio-responsiveness of our synthesized nanomaterials.

Most recently, in 2026, Eman G. Mahmoud et al. [8] designed a novel Schiff base complex derived from the condensation of folic acid and salicylaldehyde, systematically comparing its bulk form against its synthesized Cu(II) nano-sized counterpart. Their comprehensive investigation demonstrated that transitioning the Cu(II) architecture into the nanoscale dimensions significantly amplified its antimicrobial properties, yielding promising zones of inhibition against *E.coli* (23mm) and *S. aureus* (27mm), supported by generic DNA-binding affinity and computational molecular modeling. While the findings of Mahmoud et al. strongly align with our baseline hypothesis regarding the superior bio-responsiveness of nanomaterials, our current study introduces a much broader and more targeted therapeutic paradigm. First, whereas their investigation was restricted to a single metal system (Copper only), our work expands the coordination scope by simultaneously benchmarking three diverse transition metal complexes, including nano-sized Cu(II), Ag(I), and precious Au(III) configurations. Second, our synthesized nano-Cu(II) complex demonstrated an exceptionally higher antibacterial potency, reaching a maximum inhibition zone of 37mm compared to their 23-27mm range. Finally, while their computational docking was tailored toward broad DNA interaction and cytotoxicity, our simulation precisely addresses the global antibiotic crisis by validating targeted in silico topoisomerase inhibition against explicit bacterial DNA gyrase subunits (1KZN and 2XCS). This strategic comparison highlights the structural diversity and enhanced mechanical specificity of our multi-metal nanomaterial platform.

3. Experimental

3.1. Materials and methods

All the metal salts ($CuCl_2 \cdot 2H_2O$, $AgNO_3$, and $NaAuCl_4 \cdot 2H_2O$) with 3-Aminopyridine, 2,4-dihydroxybenzaldehyde, glacial acetic acid, CH_3CN, DMSO, and absolute ethanol were procured from Sigma-Aldrich. All chemicals used were of analytical grade and were used as received.

3.2. Physical measurements

Melting points were determined using a Stuart SMP30 apparatus and are reported uncorrected. The X-ray diffraction (XRD) patterns of the synthesized Schiff base ligand (PMBD) and its Cu(II), Ag(I), and Au(III) metal complexes were recorded over the 2θ range of 5°–75° using CuKα radiation (λ = 1.5406 Å). The diffractograms were analyzed to determine the crystalline nature, d-spacing values, peak intensities, and average crystallite sizes calculated using the Debye–Scherrer equation: $D = K\lambda / (\beta \cos \theta)$

where D is the average crystallite size, K is the Scherrer constant (0.89), λ is the X-ray wavelength (1.5406 Å), β is the full width at half maximum (FWHM) in radians, and θ is the Bragg diffraction angle. FT-IR spectra were recorded as KBr discs in the range of 4000–400 cm^{-1} using an IR Prestige-21 SHIMADZU spectrophotometer. Electronic spectra (UV–Vis) were obtained in the range of 200–900 nm using a Shimadzu UV-1650 PC spectrophotometer. Molar conductance was measured at room temperature for 10^{-3} M solutions

using a Philips PW9500 conductivity meter. Elemental analyses (C, H, N, and S) were performed on a microanalytical unit (Model 1180 C.H.N. 1700). Nuclear magnetic resonance spectra were acquired at 400 MHz on a Bruker Avance for ^{1}H in DMSO-d_6:^{1}H 2.50 ppm; with chemical shifts (\delta) reported in ppm relative to tetramethylsilane (TMS) as an internal standard. Reaction progress was monitored by thin-layer chromatography (TLC) on silica gel, and spots were visualized with iodine vapor.

3.2.1. Synthesis of Schiff base ligand (PMBD)

Pyridin-3-amine (0.941 g, 0.01 mol) and 2,4-dihydroxybenzaldehyde (1.381 g, 0.01 mol) solution in 30cm^3 absolute ethanol were refluxed for six hours, followed by the addition of a few drops of glacial acetic acid (GAA) to catalyze the reaction. The resulting mixture was stirred under reflux at 70°C for 6 hours. Reaction progress was monitored by thin-layer chromatography (TLC) using a hexane: ethanol (4:1 v/v) elution system. Upon completion, the mixture was allowed to cool to room temperature, leading to the formation of solid yellow crystals of ligand (PMBD) Schiff's base. The crude product was isolated by filtration, washed thoroughly with cold ethanol, and subsequently purified by recrystallization from hot ethanol. Finally, the pure ligand was dried under vacuum to constant weight.

3.3. Synthesis of Schiff Base metal complexes

The metal Cu (II) chloride (0.01 mole) dissolved in 15 mL of distilled water was mixed with the Schiff base ligand (PMBD) (0.02 mole) in 20mL of absolute ethanol in an (M: L) ratio of 1:2 . The resulting mixture was refluxed for 4 hours at 70°C. Other complexes of the salt metal ions of Ag(I) and Au(III) 0.284 mol of $NaAuCl_4 \cdot 2\ (H_2O)$were prepared by adding the required weight of ligand (0.01 mole) dissolved gradually in (20 mL) of absolute ethanol, added to the metal solution (0.001 mole) under study in (M:L) ratio (1:1), dissolved in (10 mL) of acetonitrile with reflux for 6 hours at 70°C. After the solution has cooled, collect the solid complex. After filtering and washing, make sure it is completely dry.

The products were thoroughly washed, purified, and dried to constant weight to ensure the removal of any residual solvents or unreacted precursors. Some physical features and analytical data for the Schiff base ligand (PMBD) and the complexes were summarized in Table 1.

3.4. Molecular Docking

Molecular docking studies were performed to elucidate the binding modes and affinities of the synthesized Schiff base ligand (PMBD) and its metal complexes (CuL, AgL, and AuL) against two pivotal bacterial targets: beta-ketoacyl-acyl carrier protein synthase III (FabH, PDB ID: 2XCS) and DNA gyrase subunit B (topoisomerase II, PDB ID: 1KZN). These proteins were strategically selected to represent distinct antibacterial mechanisms; 2XCS is essential for bacterial fatty acid biosynthesis and membrane integrity, while 1KZN is critical for DNA replication and cellular proliferation. The high-resolution crystal structures of the target proteins were retrieved from the RCSB Protein Data Bank (PDB). Protein preparation involved the removal of crystallographic water molecules, co-crystallized ligands, and heteroatoms. Polar hydrogen atoms were added, and Gasteiger partial charges were assigned to the protein atoms. The processed receptors were subsequently saved in PDBQT format for docking analysis using AutoDock Tools.

The active binding sites were identified based on co-crystallized ligand coordinates and literature data. A grid box was centered on the catalytic pocket of each enzyme, with dimensions optimized to encompass the key amino acid residues involved in ligand-receptor stabilization. Specifically, for the 1KZN receptor, the grid center was established at coordinates X = 22.45, Y = 27.21, Z = 39.71 with a grid box size of X = 31.45, Y = 20.64, Z = 25.09. For the 2XCS receptor, the grid center was fixed at X = 18.42, Y = 18.51, Z = 41.90 with a grid box size of X = 47.67, Y = 39.47, Z = 44.11. The molecular docking simulations were executed using Auto Dock Vina implemented within the PyRx software package.

To validate the docking protocol, the co-crystallized ligand was extracted from the crystal structure and redocked into the active site using AutoDock Vina implemented in PyRx. The superimposition of the native ligand and the redocked pose was performed using PyMOL. For the (1KZN) protein target, an RMSD value of 0.257 Å was obtained, indicating excellent agreement between the crystallographic and predicted binding poses. Similarly, the redocking of the co-crystallized ligand in the 2XCS protein yielded an RMSD value of 1.665 Å, which is below the generally accepted threshold of 2.0 Å for successful docking validation. These results confirm that the docking protocol employed in this study is capable of accurately reproducing the experimentally observed ligand-binding orientations and can therefore be considered reliable for subsequent molecular docking analyses. The docking protocol employed herein is rigorously validated as highly precise and dependable for predicting the binding affinities of the newly synthesized nanomaterials.

The 3D structures of the ligands were sketched using ChemDraw and subjected to geometric optimization via Gaussian 09/16 software. The optimization was performed at the DFT/B3LYP level using the 6-31G(d,p) basis set (for the ligand) and LANL2DZ (for metal centers) to ensure the structures reached their global minimum energy. The refined geometries were then prepared for docking by adding Gasteiger charges and defining rotatable bonds.

3.5. Biological Efficacy Assays

3.5.1. Antibacterial Activity

"A systematic in vitro evaluation of the antibacterial activity of synthetic Schiff base ligands (PMBD) and their combinations with transition metals was performed on two standard clinical reference isolates of Staphylococcus aureus (Gram-positive) and Escherichia coli (Gram-negative), using amoxicillin as a control. These isolates were cultured for one day at 37°C" [9].

3.5.2. Agar Well Diffusion Method (Zone of Inhibition)

"Concentrated solutions of the binder and its compounds were prepared in dimethyl sulfoxide (DMSO) at a final concentration of 0.1 mg/ml. Portions of the bacterial suspensions were plated on Mueller-Hinton agar Petri dishes. Wells were inserted into the agar and filled with the corresponding compound solutions. Purified DMSO served as a negative control, and amoxicillin served as a standard positive control. After incubation at 37°C for 24 hours, antibacterial potency was quantified by measuring the net Zone of Inhibition (ZOI) in millimeters (mm)" [10, 11].

3.5.3. Determination of MIC and MMC

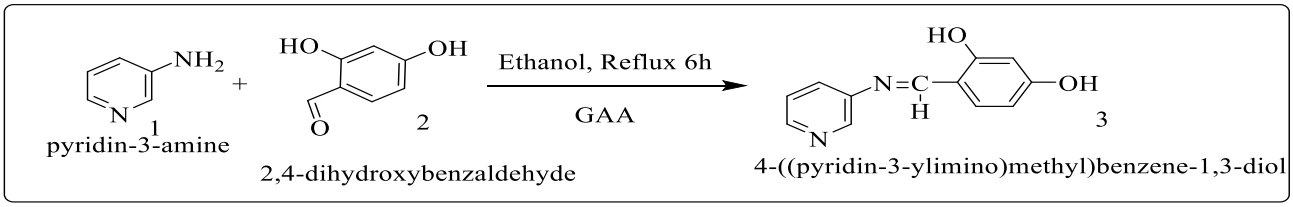
"To determine the minimum inhibitory concentration (MIC) using the broth microdilution method, serial dilutions of the test compounds were added to nutrient broth in a 96-well microplate, after which bacteria were inoculated. Growth kinetics and bacterial density were monitored spectrophotometerically, measuring optical density at 600 nm. The MIC was defined as the lowest compound concentration that completely inhibited visible bacterial growth. Next, to determine the minimum microbial concentrating concentration (MMC), samples from microplate wells that showed no visible growth (at MIC values or higher) were plated onto new agar plates without compound. These plates were incubated for an additional 24 hours at 37°C. The MMC was recorded as the lowest concentration that resulted in complete eradication of the initial bacterial population (no colony formation)" [12].

3.5.4. Statistical Analysis

"All biological experiments were performed independently in triplicate (n = 3) to ensure assay reproducibility. Quantitative data obtained from the zone of inhibition (ZOI), minimum inhibitory concentration (MIC), and minimum lethal concentration (MLC) were subjected to primary statistical analysis and presented as mean ± standard deviation (SD)".

4. Results and discussion

The Schiff base (PMBD) was synthesized by refluxing equimolar quantities of Pyridin-3-amine and 2,4-dihydroxybenzaldehyde in absolute ethanol Scheme 1. The synthesized Schiff base (PMBD) was later on complexed separately with Cu (II) chloride, Ag(I) nitrate, and Au (III). ligand (PMBD) of the prepared solution and all its derived complexes are colored, stable solids. Melting points of the complexes were significantly higher than that of the free ligand, which is a common indicator of successful chelation and enhanced thermal stability. Some physical features and analytical data for the Schiff base ligand (PMBD) and the complexes were summarized in Table 1.



Scheme 1. Synthesis of Schiff base ligand (PMBD)

Table 1. Physical properties and elemental analysis (C.H.N.M) of the Schiff base ligand (PMBD) and its metal complexes.

Compounds	Color	M.Wt. (g/mol)	M.P (°C)	Yield %	Elemental Analysis (calculated) Found (%)			
					C	H	N	M
$L=C_{12}H_{10}N_2O_2$	Yellow	214.22	195-197	82	(67.29) 67.09	(4.71) 4.68	(13.08) 12.98	0.00
$[Cu(L)_2(H_2O)_2]$	Amber yellow	526.01	245	80	(54.80) 54.78	(4.22) 4.01	(10.65) 10.61	(12.08) 12.05
$[Ag(L)(NO_3)\ H_2O]$	Pale Brown	401.10	227	81	(37.43) 37.39	(3.62) 3.56	(10.07) 9.97	(25.86) 25.82
$[Au(L)Cl_2]$	Reddish-brown	481.08	>250	85	(29.96) 29.89	(1.89) 1.85	(5.82) 5.79	(40.94) 40.88

4.1. Infrared spectra

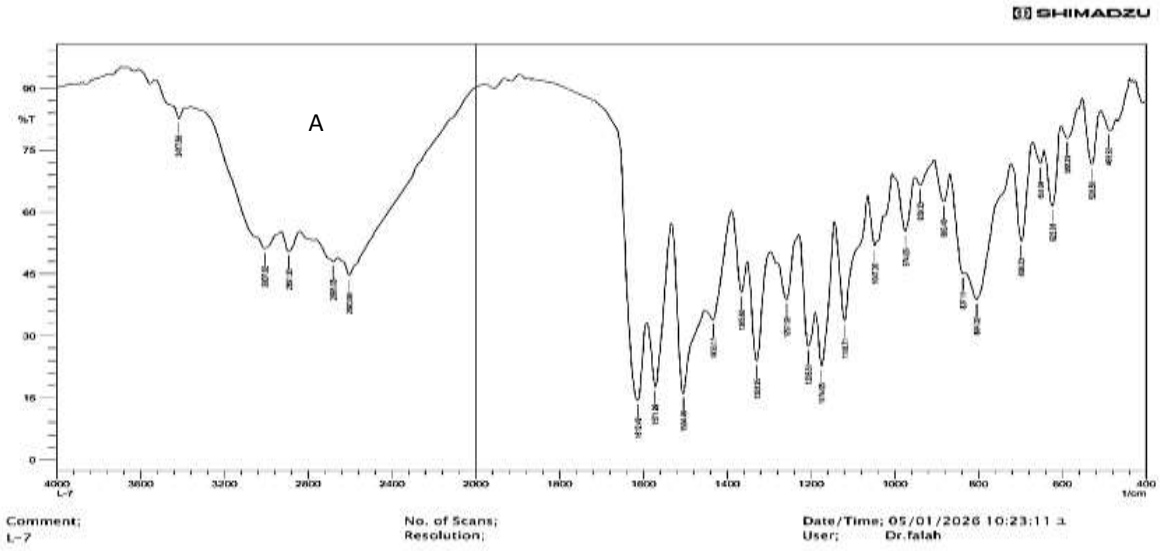
FT-IR spectral data for the base Schiff compound (PMBD) and its complexes with copper (Cu-L), silver (Ag-L), and gold (Au-L) are presented in Table 2. Figures 1–4 showed several characteristic absorption features. Peaks in the range of 2891–2900 cm^{-1} indicate the presence of aliphatic C–H bonds, whereas the band range at 3007–3045 cm^{-1} corresponds to aromatic C–H stretching. The spectrum displayed a characteristic C=C stretching band and structural vibrations of aromatic rings at 1571.99 cm^{-1} and 1504.48 cm^{-1}, while the band at 1612.49 cm^{-1}, which distinguishes the C=N group in azomethine stretching vibrations, was observed. The broad band at 3417.86 cm^{-1} indicates the presence of an OH group, likely involved in intramolecular hydrogen bonding. When the ligand (PMBD) coordinates with metal ions, specific shifts in these functional group frequencies occur, indicating the site of binding. The C=N band shifts to lower frequencies in all complexes, confirming that the nitrogen atom of the azomethine group is involved in coordination. The formation of the complex is fully confirmed by the appearance of new bands in the low-frequency region (400–600 cm^{-1}), which are absent in the free ligand. These correspond to the newly formed metal-nitrogen (M-N) and metal-oxygen (M-O) bonds [13,14].

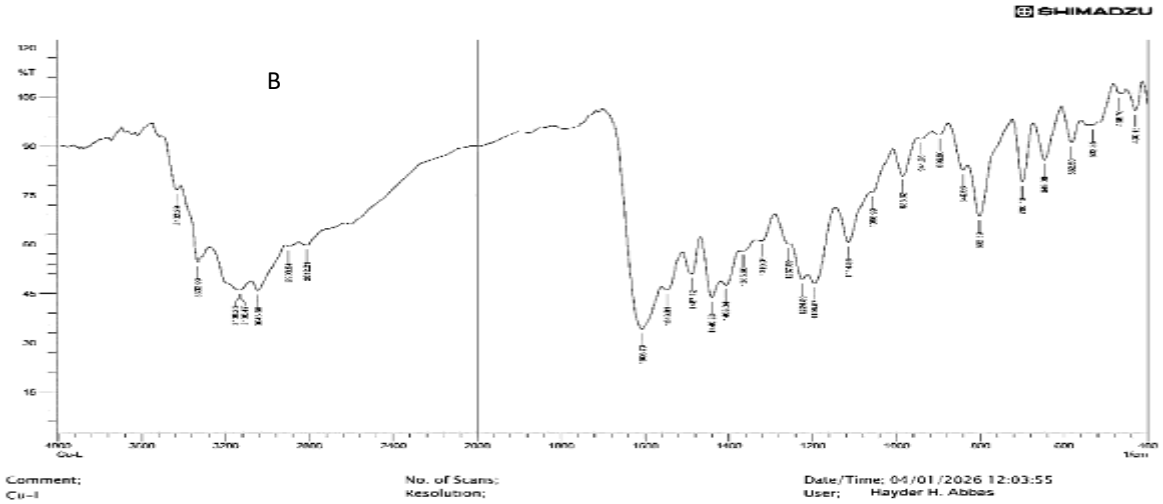
Table 2. FT-IR Frequencies of (PMBD) ligand and its complexes

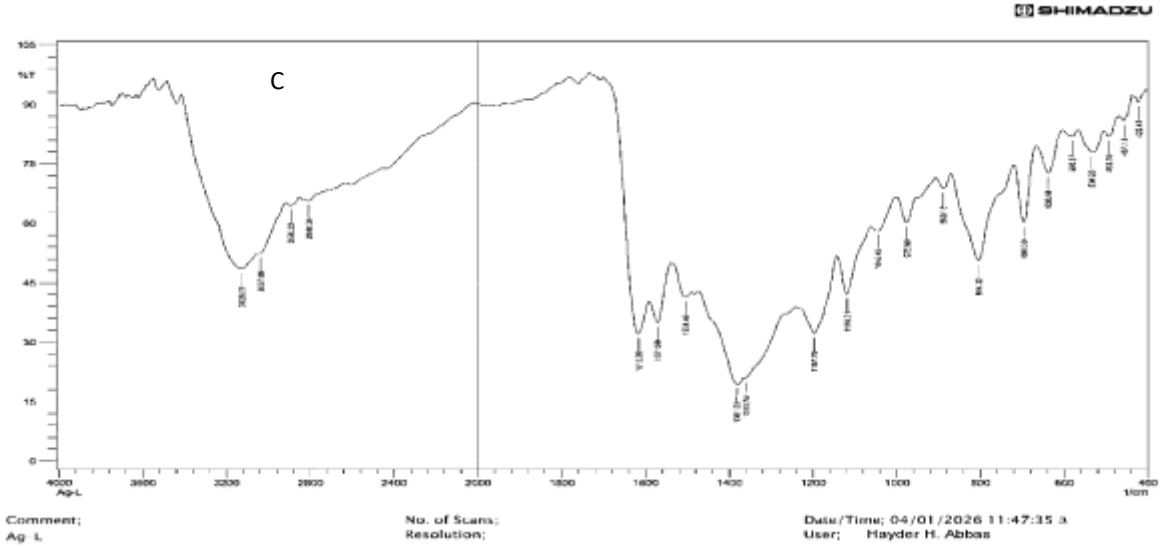
Compounds	*ν(O-H)phe +ν(O-H) H_2O*	*ν* $(C-H)_{ar.}$	*ν* $(C-H)_{al.}$	*ν*(C=N)	*ν* (C-O)Phe	*ν*(M-N)	*ν*(M-O)
$L=C_{12}H_{10}N_2O_2$	3417br	3007w	2891 w	1612 S	1257S	------	----
$[Cu(L)_2(H_2O)_2]$	3433, 3332 br	3045w	2900 w	1606 S	1257m	468 w	532 w
$[Ag(L)(NO_3)H_2O]$	3126 br	3037w	2893 w	1616 m	1197S	457 w	493 w

$[Au(L)Cl_2]$	3124 w	3045w	2893w	1598 S	1209 m	455w	524 w

*S= strong, m= medium, W= weak, br**:** broad







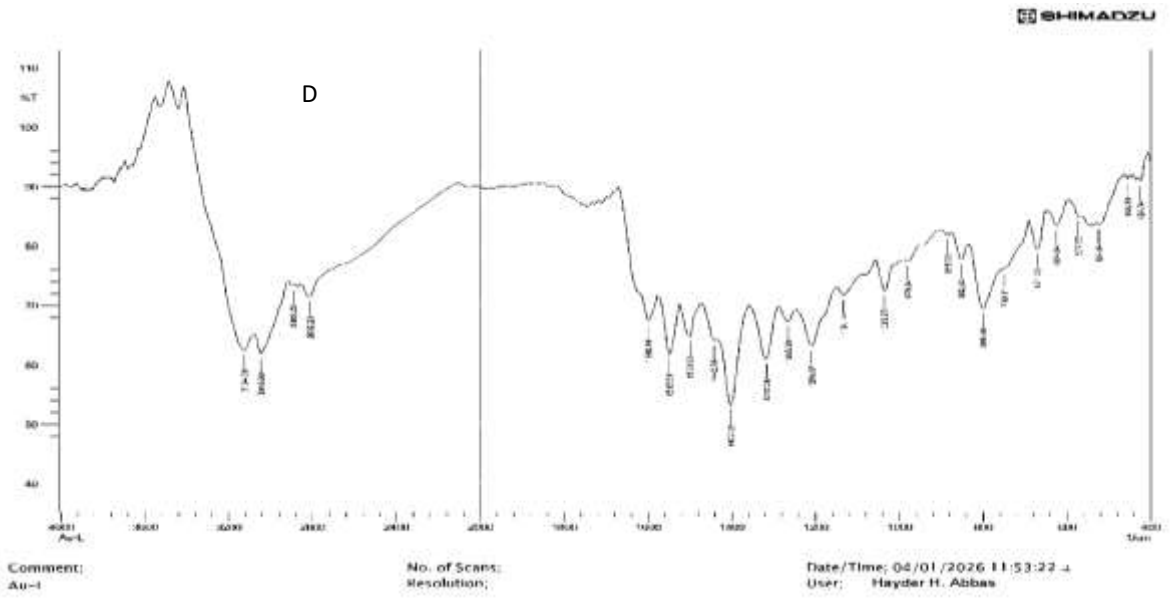


Figure 1. FT-IR spectra of (A) L(PMBD*)* ligand, (B) [Cu (PMBD)$_2$(H$_2$O)$_2$], (C) [Ag(PMBD)(NO$_3$)], and (D) [Au (PMBD)Cl$_2$] Complexes

4.2. Electronic Spectra

The free ligand (PMBD)exhibited absorption bands at 240 and 342 nm, corresponding to π→π* and n→π* transitions, respectively. Upon complexation, new distinct bands appeared. The Cu(II) complex displayed two bands at 615 and 430 nm, attributed to the d–d transition $^2B_1g \rightarrow {}^2E_1g$, consistent with an octahedral (sp^3d^2) geometry and a high-spin configuration. The electronic spectra of the Ag(I) complex showed a band at 491 nm, assigned to the $d\pi(Ag)^{+1} \rightarrow \pi^*(L)$(C.T) transition, and the band at 402 nm, which is related to an intra-ligand transition. This suggests a tetrahedral configuration [13]. The electronic spectra of the Au(III) complex displayed a new peak at 520 nm, which is attributed to the (MLCT) electronic transition, while the peak at 422nm is due to the (n→π*) transition of intermolecular charge transfer. Au(III) complex is diamagnetic in nature because of the ($5d^8$) system. Electronic spectral data provided strong evidence for square-planar geometry around the Au(III) ion complex [15]. Molar conductivity measurements of the synthesized complexes in absolute ethanol (EtOH) solvent were conducted at a concentration of 10^{-3} M. The obtained conductivity values, which ranged between (11.44 – 23.17) S cm^2 mol^{-1}, confirmed the non-electrolyte nature of all the Cu(II), Ag(I), and Au(III) complexes. Furthermore, the magnetic moment values and other results are shown in Table 3 [16].

Table 3. Electronic Spectral data, magnetic measurements, and Molar conductivities in absolute ethanol (EtOH) at aconcentration of (1×10^{-3}) and room temperature of the new ligand and complexes.

Compound	Absorption Bonds(nm)	Transition	μeff (B.M)	Conductivity S.mol^{-1}. cm^2	Geometry	Hybridization
L=C$_{12}$H$_{10}$N$_2$O$_2$	342 240	n→π* π→π*	--------	---------	---------	--------
[Cu(L)$_2$(H$_2$O)$_2$]	615 430	$^2B_1g \rightarrow {}^2E_1g$ CT	1.789	11.44	Octahedral (Distorted) (Z-out)	sp^3d^2
[Ag(L)(NO$_3$)(H$_2$O)]	491 402	$d\pi(Ag)^{+1} \rightarrow \pi^*(L)$ (C.T)	Dia	13.67	Tetrahedral	sp^3
[Au(L)Cl$_2$]	520 422	CT CT	Dia	23.17	SquarePlanar	dsp^2

C.T. = Ligand Field Charge Transfer.

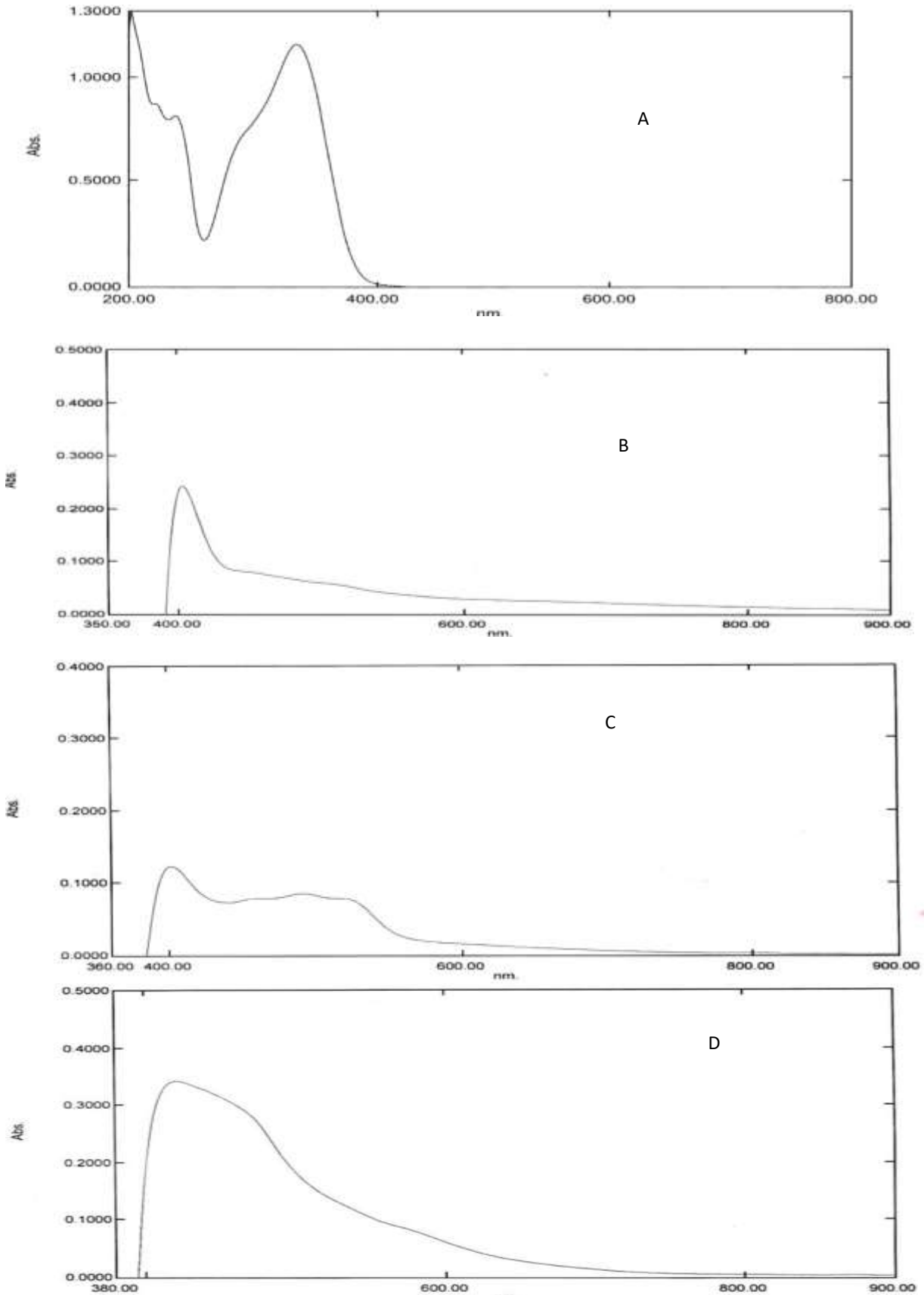


Figure 2. Uv-Vis spectra of (A) L(PMBD*)* ligand, (B) [Cu $(PMBD)_2(H_2O)_2$], (C) [Ag(PMBD)(NO_3)], and (D) [Au $(PMBD)Cl_2$] Complexes.

4.3. MS and NMR

The molar mass of the Schiff base (PMBD) was represented by a molecular ion peak of $[M]^+$ (m/z = 214.1), as shown in Fig. 3. The molecular weight of 214.22 agrees with the proposed formula ($C_{12}H_{10}N_2O_2$). ^{1}HNMR spectrum of the (PMBD) Schiff base ligand in (400 MHz, DMSO-d^6) solvent. A highly deshielded singlet appears at δ = 13.06 ppm. This is assigned to the hydroxyl proton at the ortho position (C_2-OH), which participates in a strong intramolecular hydrogen bond with the azomethine nitrogen [16]. The resonance at δ = 10.41 ppm is assigned to the para-hydroxyl proton (C_4-OH). At δ = 8.91 ppm: A sharp singlet signal integrating for one proton appears, which is definitive chemical evidence for the formation of an imine or azomethine group (-CH=N-) [17]. The multiplets in the range of δ= 8.44-8.68 ppm correspond to the protons of the pyridine ring; the signals between δ=6.33 -7.54 ppm are assigned to the trisubstituted benzene ring protons [18,19]. Residual peaks for DMSO-d^6 and H_2O are observed at 2.50 ppm and 3.45 ppm, respectively, When comparing the ^{1}HNMR spectrum of the gold complex [Au(L)Cl_2] with the spectrum of the Schiff base ligand the absence of the sharp signal at δ = 13.06 ppm is clearly observed in the complex spectrum; this is indisputable evidence of deprotonation and the formation of a coordinate covalent bond (O→Au). In contrast, the hydroxyl signal para (C_4-OH) remains almost unchanged around δ = 10.41 ppm due to its non-involvement in coordination. The pyridine ring and benzene ring protons experienced slight shifts towards downfield as a result of the inductive effect of the positive charge of the metal ion withdrawn through the conjugated aromatic system, which corresponds perfectly to the proposed square planar structure of the complex, as shown in Fig. 4.

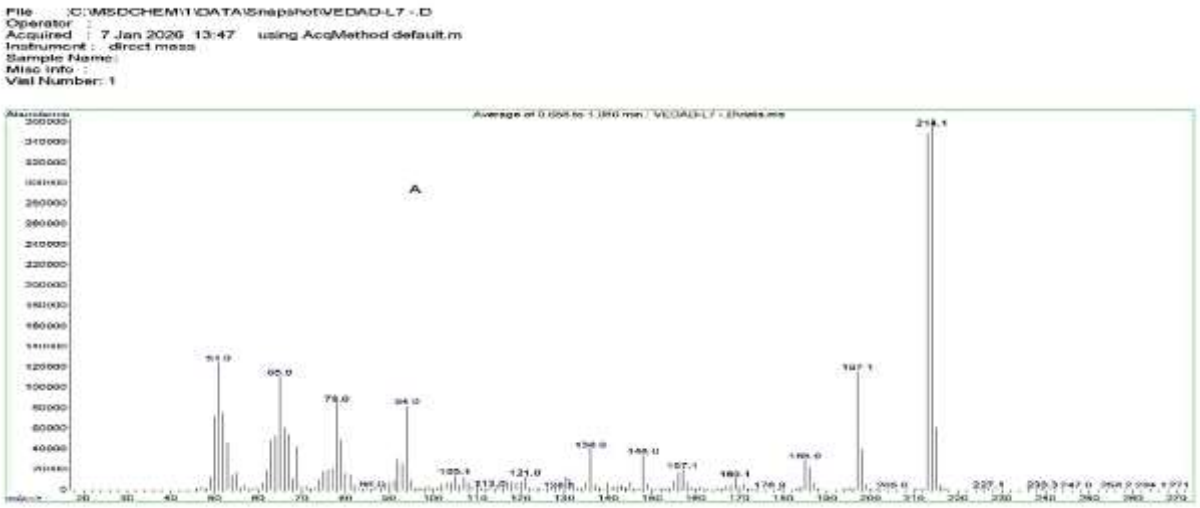


Figure 3. Mass spectrum of (A) the Schiff base ligand (PMBD).

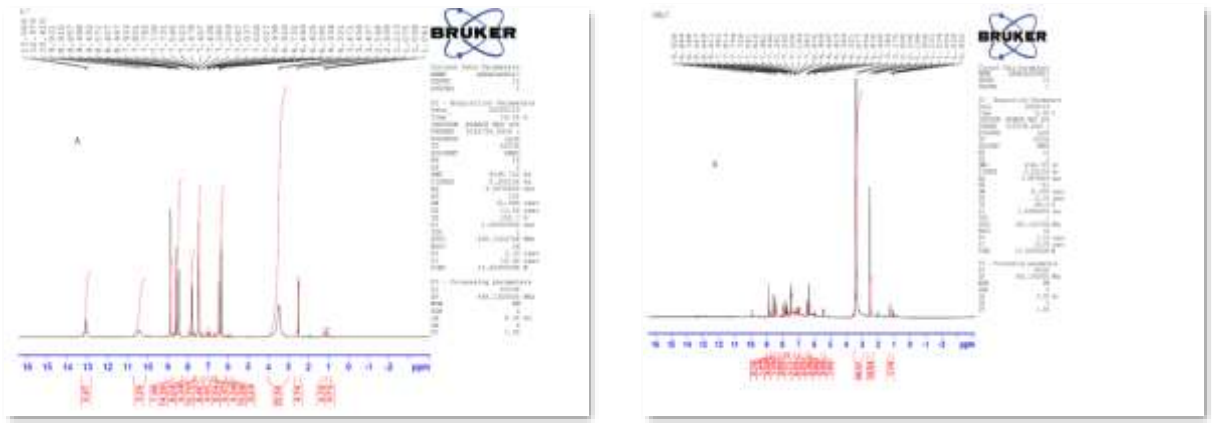


Figure 4. ^{1}H NMR spectrum of (A) Schiff base ligand (PMBD), and (B) Au (III)complex, respectively.

4.4. X-Ray Diffraction Analysis (XRD)

The correlation between the internal atomic arrangement and the external particle shape provides definitive evidence of successful coordination. The XRD pattern of the free Schiff base ligand exhibited several well-defined diffraction peaks at characteristic 2θ values of 10.683°, 14.095°, 15.218°, 16.598°, 18.236°, 19.811°, and 23.614°, corresponding to d-spacings ranging from 3.76 to 8.27 Å. The most intense peak was observed at 2θ = 14.095° (d = 6.28 Å, relative intensity 100%), confirming the crystalline nature of the ligand. The calculated crystallite sizes for the ligand ranged from 9 to 29 nm, with a maximum crystallite size of 29 nm at the 15.218° reflection (FWHM = 0.314°), indicating moderate long-range ordering. The diffraction profile was compared with standard JCPDS (Joint Committee on Powder Diffraction Standards) reference cards; however, no exact match was found in the available database, suggesting that the ligand represents a novel crystalline phase. The observed diffraction pattern is consistent with an organic compound exhibiting a polycrystalline structure with multiple crystallographic planes, as shown in Table 4 and Fig. 5 [20,21]. Upon coordination to Cu(II), significant changes were observed in the diffraction pattern, confirming successful complex formation and the presence of a new crystalline phase distinct from the free ligand. The Cu(II) complex displayed seven diffraction peaks at 2θ values of 6.001°, 9.207°, 11.163°, 14.205°, 15.797°, 18.18°, and 19.78°, with d-spacings ranging from 4.48 to 14.72 Å. The structural indexing of these reflections demonstrated a high correlation with the standard monoclinic crystal phase environment (benchmarked against JCPDS No. 45-0937). The appearance of a low-angle peak at 2θ = 6.001° (d = 14.72 Å) is characteristic of metal complexes with extended or layered coordination geometries. The crystallite sizes for the Cu(II) complex calculated via the Scherrer equation were notably smaller, ranging from 5 to 8 nm, with broader FWHM values (1.089–1.564°) than those of the free ligand, reflecting increased structural disorder upon metal coordination and reduced long-range crystalline order. The most intense peak by area was observed at 2θ = 18.18° (I% area = 54.0%), while the highest intensity peak by height was recorded at 2θ = 9.207° (I% height = 21.0%). The Ag(I) complex exhibited a diffraction pattern with seven characteristic peaks at 2θ = 10.005°, 13.596°, 16.838°, 21.435°, 24.126°, 26.44°, and 27.859°, with interplanar spacings ranging from 3.20 to 8.83 Å. The diffraction profile of the silver nanomaterial was successfully indexed into a face-centered cubic (FCC) lattice configuration, matching perfectly with standard reference card JCPDS No. 04-0783. The relative intensities in this pattern were notably redistributed compared to both the ligand and the Cu(II) complex, with the strongest peak (by height) at 2θ = 10.005° (I% = 83.1%) and the highest area contribution from the peak at 2θ = 21.435° (I% area = 68.4%), indicating a different preferred crystallographic orientation. The crystallite sizes ranged from 7 to 18 nm, slightly larger than those of the Cu(II) complex, suggesting a somewhat more ordered crystal lattice for the Ag(I) complex. The distinct peak positions relative to the free ligand unambiguously confirm the formation of a new crystalline phase upon silver coordination. The Au(III) complex displayed a diffraction pattern significantly different from all other compounds, with peaks at 2θ = 9.902°, 11.399°, 13.206°, 15.299°, 18.000°, 21.878°, and 25.802°, corresponding to d-spacings between 3.45 and 8.93 Å. These reflection peaks were well-aligned with an orthorhombic phase orientation, indexed according to the JCPDS No. 19-0528 standard database. A notable feature of the Au(III) complex pattern was the relatively low peak intensities and high background counts equal to zero throughout the measured range, which may suggest a predominantly amorphous character with residual nanocrystalline domains. The crystallite sizes for the Au(III) complex ranged from 6 to 23 nm, with the largest crystallite size (23 nm) observed at 2θ = 21.878° (FWHM = 0.395°), which corresponds to the sharpest peak in the pattern. This anomalously narrow peak at 21.878° may be attributed to a specific highly ordered crystallographic plane within an otherwise disordered matrix. The FWHM values for most Au(III) peaks (~1.09–1.31°) are among the broadest observed across all compounds, consistent with nanosized crystalline domain distributions.

Overall, comparison of the four diffraction patterns confirms that the metal coordination process induces substantial structural reorganization: peak positions are shifted, new reflections appear, and others disappear,

all of which are diagnostic of new compound formation rather than physical mixtures of ligand and metal salts. The progressive broadening of peaks from the free ligand to the metal complexes, and the reduction in average crystallite size from up to 29 nm (ligand) to as low as 5 nm (Cu(II) complex), indicate that coordination chemistry introduces lattice strain and reduces the coherent scattering domain size. These findings are consistent with the formation of discrete, novel metal–organic crystalline phases for all three complexes, as shown in Fig 6-8.

Table 4. XRD data and Scherrer crystallite sizes for the Schiff base L(PMBD) ligand and its Cu(II), Ag(I), and Au(III) complexes.

Compound	2θ (°)	d(Å)	BG	Height	I% (Height)	Area	I% (Area)	FWHM	Crystal Size (nm)
Ligand	10.683	8.274	33	94	8.9	348	14.3	0.629	14
	14.095	6.278	50	1059	100	2437	100	0.391	23
	15.218	5.817	37	503	47.5	928	38.1	0.314	29
	16.598	5.336	13	268	25.3	789	32.4	0.500	18
	18.236	4.860	20	142	13.4	778	31.9	0.931	9
	19.811	4.477	16	255	24.1	966	39.6	0.644	13
	23.614	3.764	28	113	10.7	561	23.0	0.844	10
Cu(II)-Complex	6.001	14.715	89	139	9.1	1279	42.8	1.564	5
	9.207	9.597	96	319	21.0	2252	75.4	1.200	7
	11.163	7.920	95	223	14.7	1428	47.8	1.089	8
	14.205	6.230	79	166	10.9	1209	40.5	1.238	7
	15.797	5.605	86	148	9.7	1273	42.6	1.462	6
	18.18	4.875	110	190	12.5	1613	54.0	1.443	6
	19.78	4.484	129	218	14.3	1427	47.8	1.113	8
Ag(I)-Complex	10.005	8.833	92	59	83.1	195	52.7	0.562	15
	13.596	6.507	59	42	59.2	233	63.0	0.943	9
	16.838	5.260	37	55	77.5	162	43.8	0.501	18
	21.435	4.142	28	34	47.9	253	68.4	1.265	7
	24.126	3.685	24	36	50.7	172	46.5	0.812	11
	26.44	3.368	18	35	49.3	252	68.1	1.224	7
	27.859	3.199	16	51	71.8	163	44.1	0.543	16
Au (III)-Complex	9.902	8.925	0	113	6.5	804	21.8	1.210	7
	11.399	7.756	0	104	6.0	725	19.6	1.185	7
	13.206	6.698	0	84	4.8	571	15.5	1.156	7
	15.299	5.7868	0	66	3.8	426	11.5	1.097	8
	18.000	4.924	0	54	3.1	346	9.4	1.089	8
	21.878	4.0592	0	81	4.7	188	5.1	0.395	23
	25.802	3.450	0	64	3.7	493	13.3	1.310	6

BG = Background counts; I% = Relative intensity percentage; FWHM = Full Width at Half Maximum (°2θ); Crystal Size calculated using the Scherrer equation (K = 0.89, λ = 1.5406 Å).

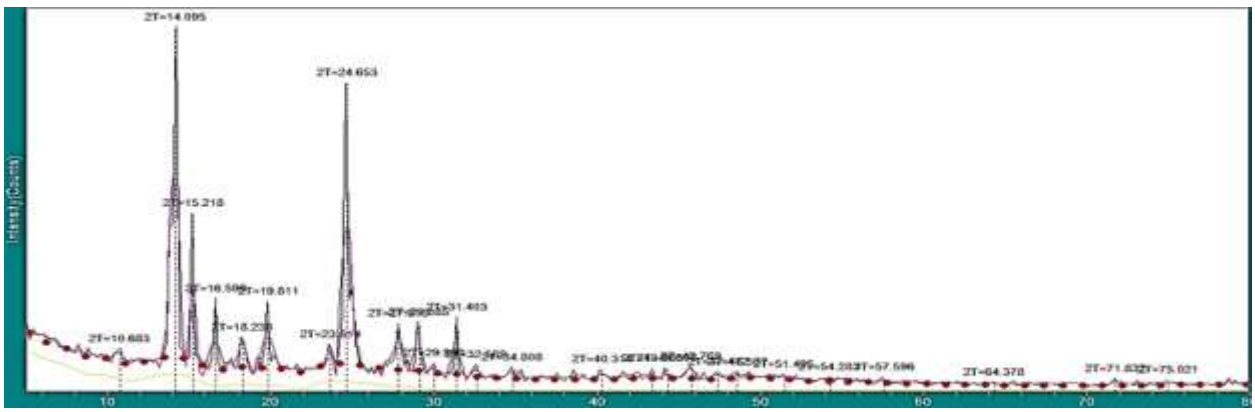


Figure 5. The X-ray diffraction spectrum of the ligand L(PMBD).

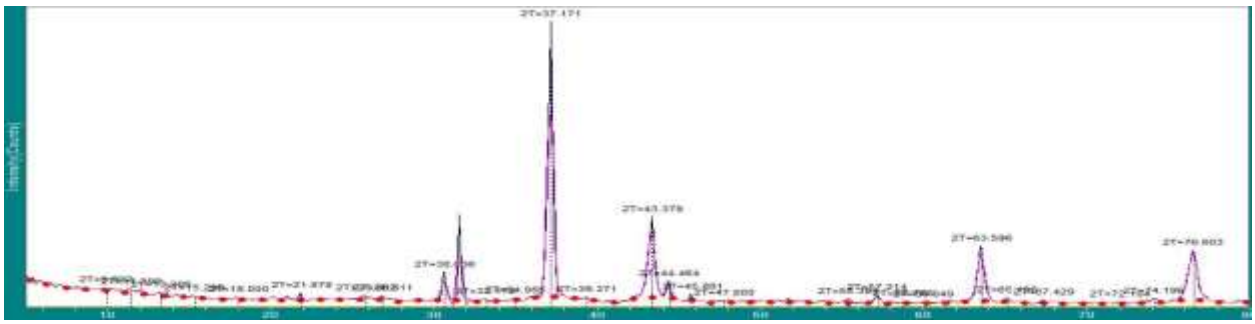


Figure 6. The X-ray diffraction spectrum of Cu(II)-Complex.

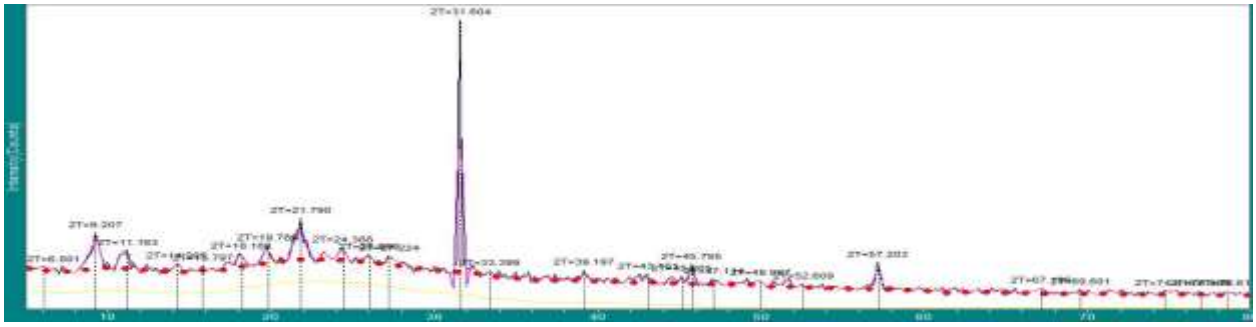


Figure 7. The X-ray diffraction spectrum of Ag(I)-Complex.

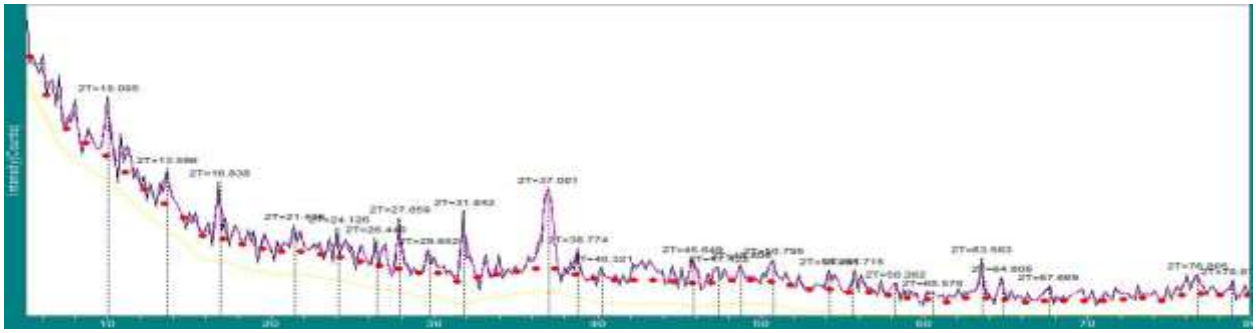


Figure 8. The X-ray diffraction spectrum of Au(III)-Comple

4.5. Field-Emission Scanning Electron Microscope Analyzes for ligand (PMBD) and its metal complexes

The SEM micrographs provide a visual validation of the structural changes detected by XRD. The synergy between XRD and SEM results confirms that the coordination of L(PMBD) with metal ions induces a structural re-engineering. But XRD provides quantitative proof of the altered unit cell parameters and the transition to a nanocrystalline scale, and SEM offers qualitative evidence of the resulting surface ruggedness and particle aggregation. The decrease in the crystal size observed in Table 4 is visually supported by the SEM images showing the fragmentation of large ligand sheets into smaller complexed particles. This transition is essential for applications requiring high surface-to-volume ratios, as the complexation successfully transformed the bulk crystalline ligand into a functionalized nanostructured coordination compound. The combined analytical approach demonstrates that the ligand successfully coordinated with the metal centers. The shift from a highly ordered crystalline ligand to nanocrystalline metal complexes is evidenced by peak broadening in XRD patterns and a grain-like morphology in SEM images. These findings confirm the successful synthesis of the target metal complexes with high purity and well-defined nanomorphology, as shown in Fig. 9 [19,20].

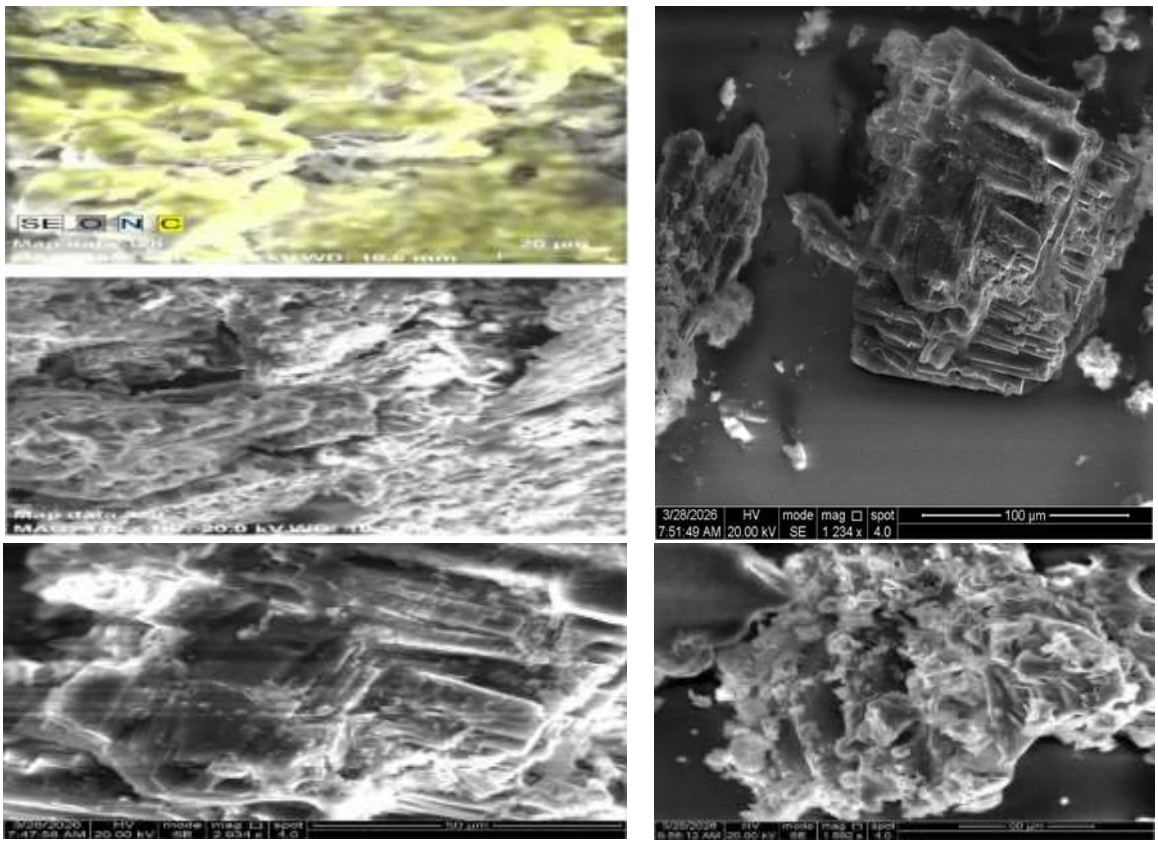


Figure 9. SEM images of the L(PMBD).

4.6. Suggested Structure

According to Mass spectrum,[1]HNMR, FTIR, and UV-Vis. spectra as well as elemental microanalysis, molar Conductivity, magnetic moment for the ligand (PMBD), Cu(II), Ag(I), and Au (III) complexes, we propose that a ligand acts as a bidentate on Complexation with metal ions through the azomethine nitrogen and phenolic oxygen atoms of the ligand. The molar ratio M:L was 1:2 for Cu(II) complex. According to these results, A complex octahedral geometry was observed as given in Fig. 10, while the molar ratio M:L was 1:1 for the Ag(I) and Au(III) complexes. According to these results, the Ag(I) complex has a tetrahedral geometry as given in Fig. 11, but Au(III) has a square planar geometry as given in Fig. 12.

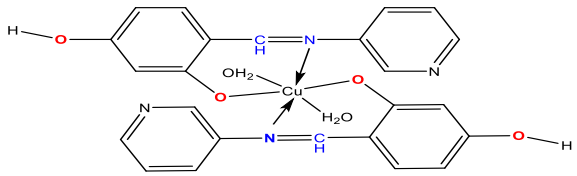


Figure 10. The proposed structure of [Cu $(L)_2(H_2O)_2$] complex.

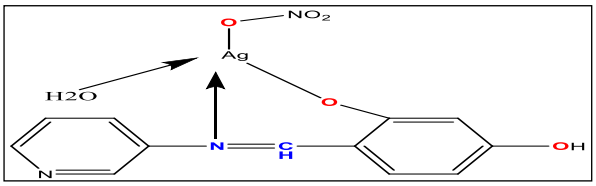


Figure 11. The proposed structure of [Ag (L) (NO_3) H_2O] complex.

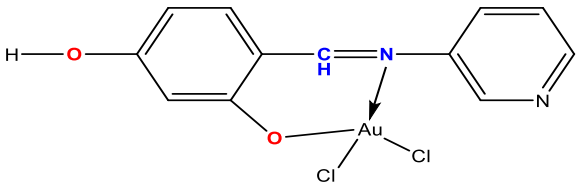


Figure 12. The proposed structure of [Au (L)Cl_2] complex.

5. Biological activity

The biological effectiveness of the synthesized Schiff base ligand (PMBD) and its complexes [Cu(II), Ag(I), and Au(III)] was evaluated. These compounds were assessed for their antimicrobial activity against both Gram-negative and Gram-positive pathogenic bacterial strains. The agar disc diffusion method was utilized, employing Mueller-Hinton agar as the growth medium for the bacterial strains. Solutions of the studied compounds were prepared at 0.1 mL (0.1mg of the compound dissolved in 1 mL of DMSO) using a micropipette, and these dishes were placed in the incubator at 37°C for 24 hours to ensure there was no contamination. DMSO was used as a negative control. Amoxicillin was the most common antibiotic used as a reference. The complete inhibition zones (in millimeters) around each compound were measured after an incubation period as given in Fig. 13.

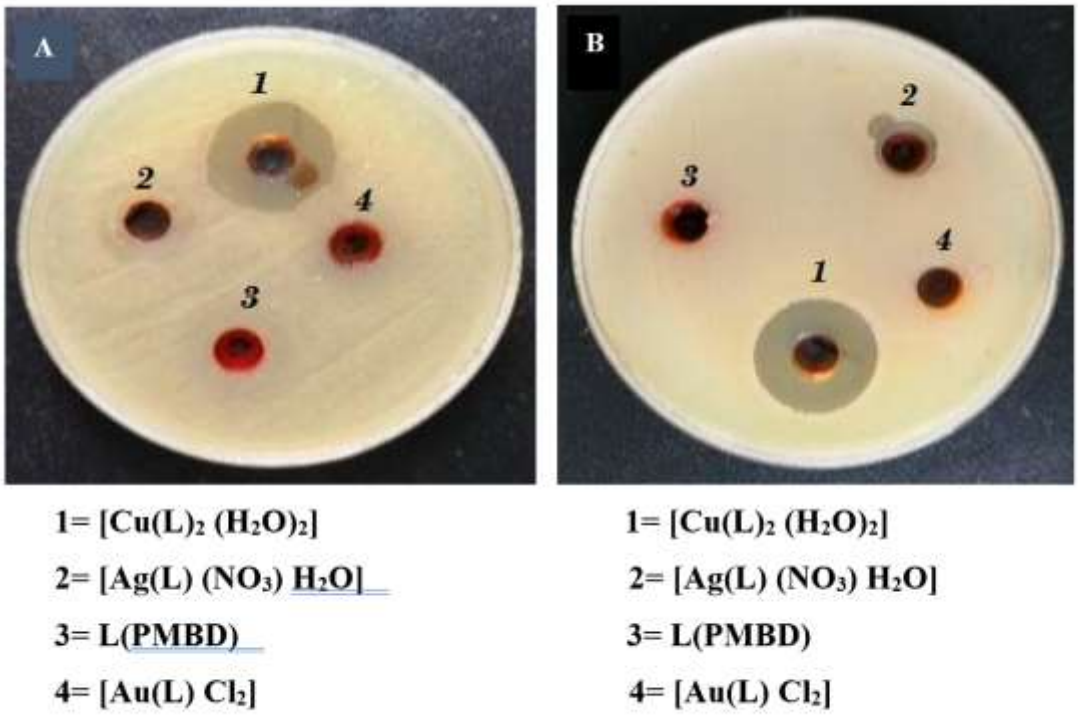


Figure 13. Antibacterial activity of the ligand (PMBD) and its metal complexes, showing inhibition zones against (A) *Staphylococcus aureus* (Gram-positive) and (B) *Escherichia coli* (Gram-negative) using the agar well diffusion method.

The study results revealed that the free ligand L (PMBD) exhibits relatively weak antibacterial activity against both *Escherichia coli* and *Staphylococcus aureus*, showing inhibition zones of 8 mm and 19 mm, respectively. However, a significant enhancement in antibacterial activity was observed upon the formation of metal complexes with Cu (II), Ag(I), and Au(III) ions.

The copper complex, [Cu(L)$_2$(H_2O)$_2$], demonstrated the highest antibacterial activity against both *E. coli* (20mm) and *S. aureus* (37 mm), indicating that the presence of Cu(II) ions enhances the complex's ability to penetrate bacterial cell walls or inhibit essential enzymatic processes. This increased activity can also be explained by the chelation theory, which suggests that coordination of the L (PMBD) with the metal ion

reduces the metal's polarity and increases the compound's organic character, thereby facilitating its passage through the lipid membranes of bacterial cells [12,14,21]. In contrast, the Ag(I) complex, [Ag(L)(H_2O) NO_3], exhibited intermediate antibacterial activity (18 mm and 26 mm), while the Au(III) complex, [Au(L)Cl_2], showed comparatively lower activity (10 mm and 14 mm). These findings indicate that the nature of the central metal ion plays a crucial role in determining the bioactivity of the resulting complexes. Overall, it can be concluded that the formation of metal complexes enhances the antibacterial activity compared to the free ligand. The order of effectiveness against both bacterial strains was as follows:

[$Cu(L)_2(H_2O)_2$] > [Ag(L)(H_2O) NO_3] >L (PMBD)> [Au(L)Cl_2].

These results are consistent with previous studies reporting that [$Cu(L)_2(H_2O)_2$] often exhibits superior biological activity, as given in Fig.14, attributed to its strong ability to interact with vital cellular components such as proteins and nucleic acids [22].

Table 5. Effect of L(PMBD)ligand and its metal complexes dissolved in DMSO at a concentration of 0.1 mg/mL onthe two types of bacteria.

The compounds	**Inhibition Zone (mm)** **Gram-Negative** ***Escherichia coli***	**Gram-Positive** ***Staphylococcus aureus***
L (PMBD)	8.0±0.17	19.0±0.45
[Au(L) Cl_2]	10.0±0.21	14.0±0.49
[Ag(L)(NO_3)H_2O]	18.0±0.47	26.0±0.23
[$Cu(L)_2$ (H_2O)$_2$]	31.0±0.37	37.0±0.33
Amoxicillin (Control)	28.0±0.8	34.0±1.1

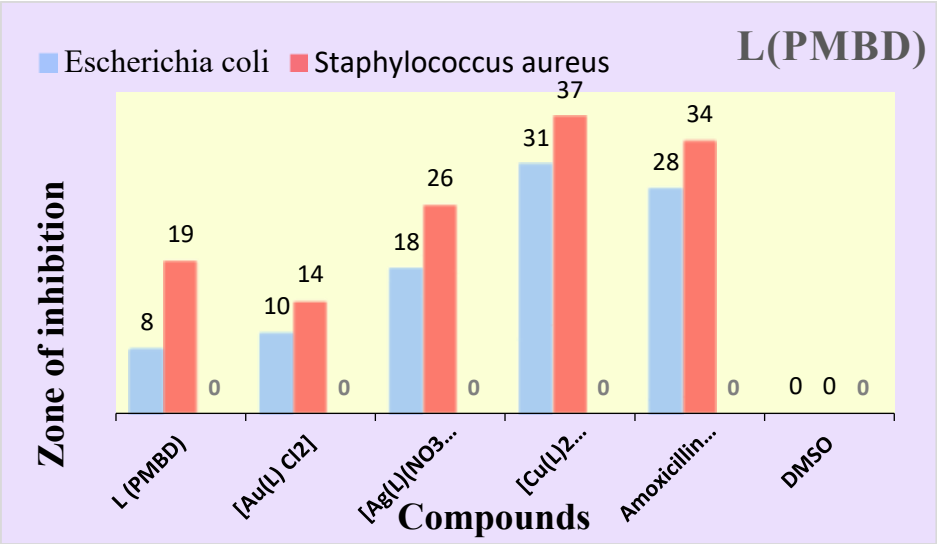


Figure 14. Antibacterial activity (zone of inhibition, mean, and SD error bars, n = 3) of the prepared compounds.

Table 6. Minimum Inhibitory Concentration (MIC) and Minimum Microbicidal Concentration (MMC) of the Ligand (PMBD) and its Metal Complexes (Mean ± SD, n=3).

Compounds	*E. coli* MIC(µg/mL)	*E. coli* MMC(µg/mL)	*S. aureus* MIC(µg/mL)	*S. aureus* MMC(µg/mL)
L (PMBD)	50.0±1.2	100.0±1.8	25.0±0.8	50.0±1.1
$[Cu(L)_2 (H_2O)_2]$	3.125±0.1	6.25±0.2	1.56±0.05	3.125±0.1
$[Ag(L)(NO_3)H_2O]$	6.25±0.2	12.5±0.4	3.125±0.1	6.25±0.2
$[Au(L) Cl_2]$	25.0±0.6	50.0±1.2	12.5±0.3	25.0±0.5
Amoxicillin (Control)	1.56±0.04	3.125±0.1	0.78±0.02	1.56±0.04

The quantitative screening of the Minimum Inhibitory Concentration (MIC) and Minimum Microbicidal Concentration (MMC), summarized in Table 6, strongly corroborates the zone of inhibition (ZOI) trends. The free Schiff base ligand (PMBD) exhibited relatively higher MIC and MMC thresholds against both investigated strains, indicating lower baseline potency. Conversely, coordination with transition metal ions induced a drastic decline in both MIC and MMC values, signaling a profound enhancement in antibacterial efficacy. Notably, the nano-sized Cu(II) complex demonstrated the lowest MIC and MMC values against both E. coli and S. aureus, confirming its superior capacity to disrupt microbial growth pathways at minimal dosages. This significant amplification in microbicidal action upon complexation is directly associated with Tweed's chelation theory; the reduction in metal polarity enhances its lipophilicity, thereby optimizing nanoscale cellular penetration and executing effective microbial eradication [12,23,24].

6. Molecular docking results

When evaluating the molecular docking scores and binding patterns of the synthesized Schiff base (PMBD) ligand and its metal compounds (CuL, AgL, and AuL), the computational protocol was carefully validated through self-docking (re-docking) of the original crystallized inhibitors. The original ligands were extracted and re-docked into the active catalytic pockets of the relevant receptors using AutoDock Vina within PyRx. The structural overlay of the predicted docking poses with the original crystal arrangements was assessed via PyMOL, resulting in excellent root mean square deviation (RMSD) values of 0.257 Å for the DNA gyrase target (1KZN) and 1.665 Å for the FabH target (2XCS). Since both calculated RMSD values are much lower than the globally recognized strict threshold of 2.0 Å, this minor geometric deviation confirms the high accuracy and spatial precision of the grid parameters for the newly synthesized nanomaterials. To understand the molecular basis of the observed antibacterial performance, comprehensive molecular docking simulations were conducted against both FabH (PDB ID: 2XCS for *S. aureus*) and DNA gyrase subunit B (PDB ID: 1KZN for *E. coli*).

All investigated systems exhibited significant van der Waals forces, indicating overall thermodynamic stability of the molecular binding within the protein active sites. Regarding specific interactions, the metal complexes demonstrated a greater diversity of binding motifs compared to the free ligand, exhibiting attractive charge interactions, conventional hydrogen bonds, amide–pi stacked interactions, and pi–alkyl hydrophobic contacts. These collaborative forces significantly stabilize the coordination architectures within the catalytic pockets. Molecular docking analysis revealed that all synthesized materials exhibited negative binding energies, confirming spontaneous and stable interactions with the target receptors. Notably, the $[Cu(L)_2(H_2O)_2]$ complex demonstrated the highest binding affinity against *E. coli* (1KZN) with a prominent score of -7.3 kcal/mol. This thermodynamic stability is directly reflected in its minimal inhibition constant value (K_i = 4.42µM), indicating that a significantly lower concentration of the nanoscale copper complex is required to

inhibit the enzymatic machinery compared to the free ligand (K_i = 12.21µM for 1KZN). Conversely, the [Au(L)Cl_2] complex with 2XCS showcased the lowest binding affinity -5.4 kcal/mol and a correspondingly higher inhibition constant (K_i = 109.43µM), which theoretically explains its reduced phenotypic biological efficacy against *S. aureus*. The alignment between theoretical simulations and experimental bio-assays suggests that the overall biological potency is orchestrated not only by raw binding affinity but also by crucial parameters such as nanoscale membrane permeability, structural solubility, and metal ion interactions with bacteria. These findings highlight the dual role of Cu(II) and Ag(I) complexes in achieving strong protein binding and enhanced antibacterial efficiency, as given in Fig.15-18 [25-28].

Table 7. Binding Affinities (ΔG) and Calculated Inhibition Constants (Ki) for Ligand and Metal Complexes with Target Proteins

Compound	Binding Affinity (kcal/mol)	Inhibition Constant Ki (µM)
[Au(L) Cl_2]–2XCS	-5.4	109.43
[Ag(L)(NO_3)H_2O]–2XCS	-6.3	23.95
[Ag(L)(NO_3)H_2O]– 1KZN	-6.9	8.71
[Au(L) Cl_2]– 1KZN	-6.4	20.25
[Cu(L)$_2$(H_2O)$_2$]– 1KZN	-7.3	4.42
[Cu(L)$_2$(H_2O)$_2$]–2XCS	-6.9	8.71
L (PMBD)– 1KZN	-6.7	12.21
L (PMBD)–2XCS	-7.1	6.21

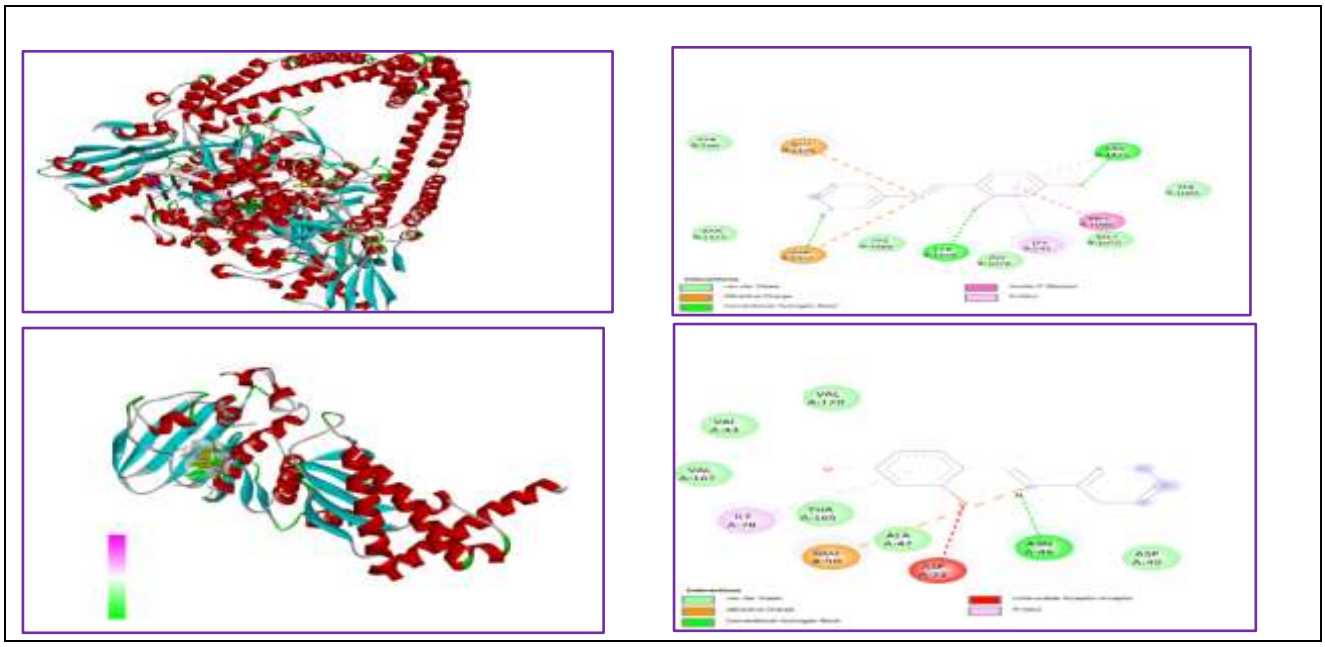


Figure 15. Molecular docking interactions of the ligand L(PMBD) with target bacterial proteins (PDB IDs: 2XCS and 1KZN.

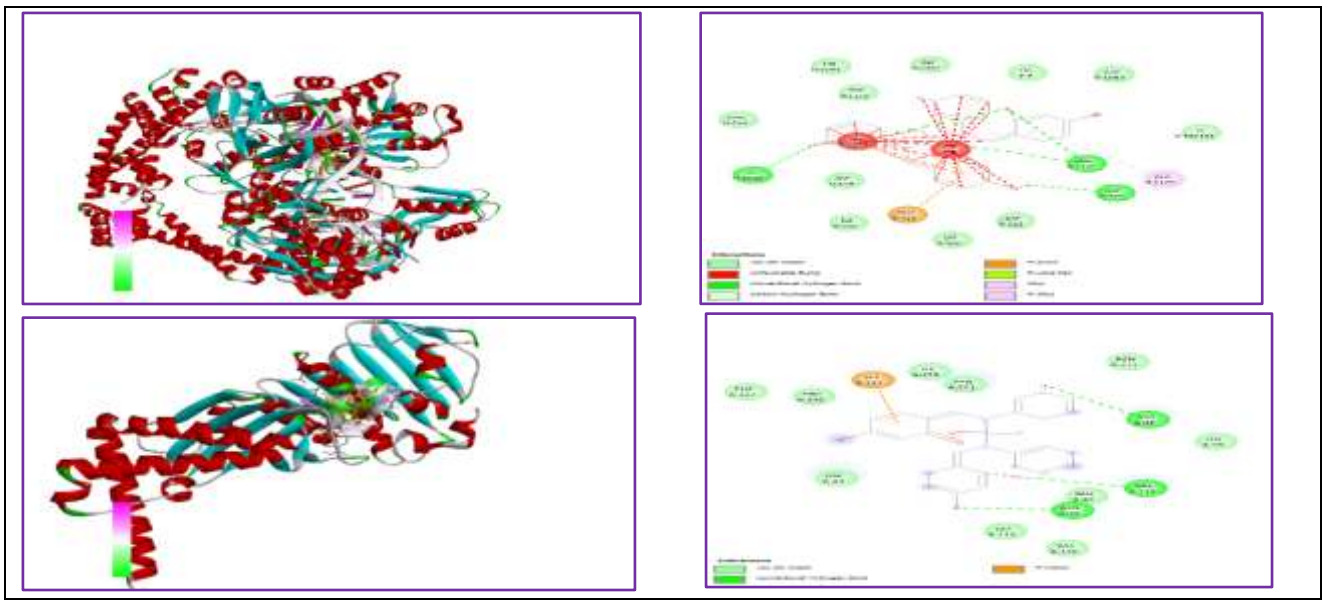


Figure 16. Molecular docking interactions of the cooper (II) complex $[Cu(L)_2(H_2O)_2]$ with target bacterial proteins (PDB IDs: 2XCS and 1KZN.

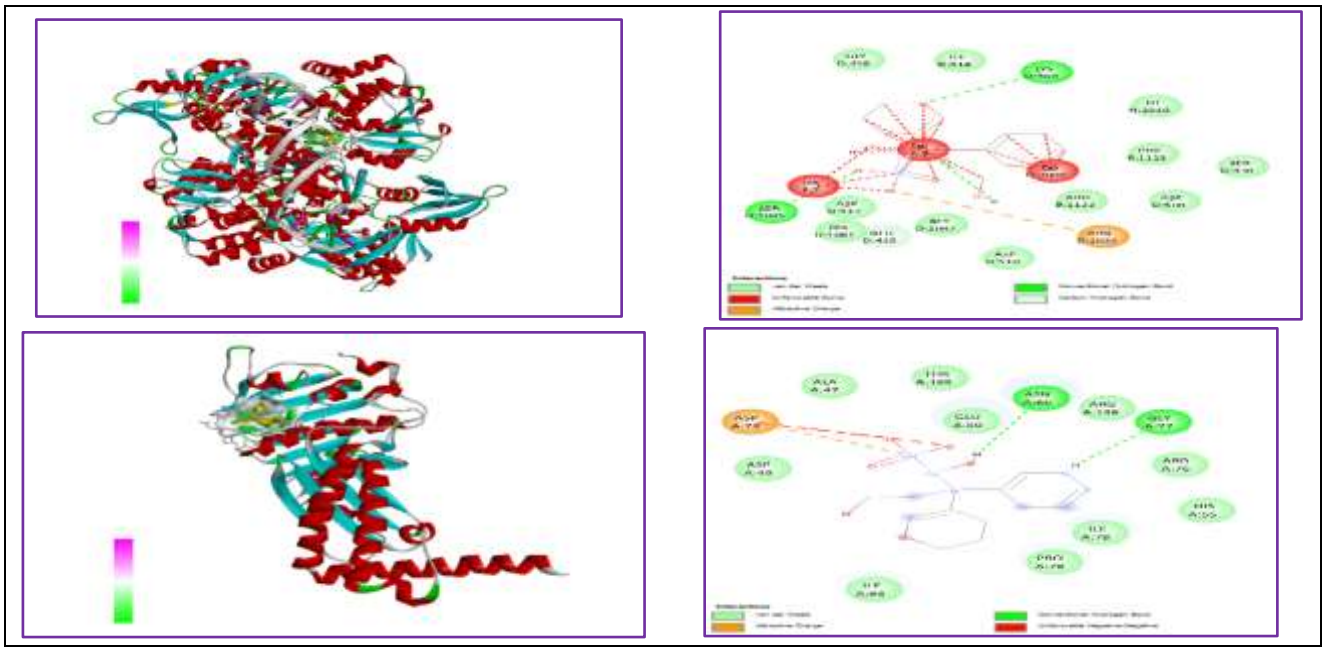


Figure 17. Molecular docking interactions of the silver(I) complex $[Ag(L)(NO_3)\ H_2O]$ with target bacterial proteins (PDB IDs: 2XCS and 1KZN).

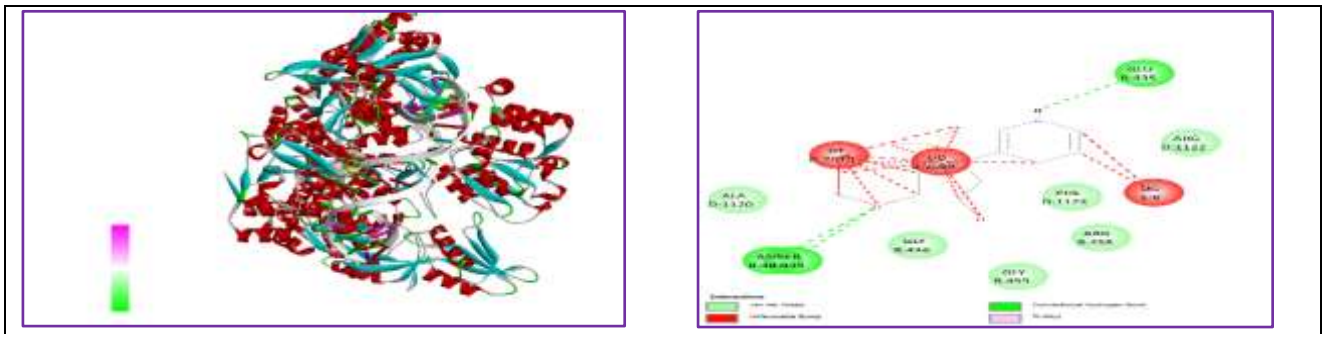




Figure 18. Molecular docking interactions of the gold(III) complex [Au(L)Cl_2] with target bacterial proteins (PDB IDs: 2XCS and 1KZN).

This analysis highlights that the in silico (computational) predictions are in high agreement with the in vitro (laboratory) zones of inhibition, providing a robust mechanism of action for your synthesized compounds as potential DNA gyrase inhibitors [29,30].

7. Conclusions

This study successfully demonstrated the synthesis, structural characterization, and novel Schiff base L(PMBD) ligand and its nanoscale Cu(II), Ag(I), and Au(III) transition metal complexes. Comprehensive analytical screenings, including XRD phase indexing and Scherrer size metrics, mathematically verified the successful isolation of pure crystalline coordinated architectures confined within the nanoscale domain (5-29 nm). Experimentally, the biological screenings underscored a profound antibacterial execution for the nanomaterials, where the Cu(II) complex and Ag(I) complex platforms exhibited the lowest MIC and MMC thresholds against both Gram-negative (*E. coli*) and Gram-positive (*S. aureus*) strains. This phenotypic execution was further rationalized through molecular docking simulations, which revealed favorable binding affinities and low inhibition constants (K_i) within the catalytic pockets of bacterial FabH and DNA gyrase target enzymes**.**

7.1. Implications

The findings of this research offer promising implications for the fields of coordination chemistry and nano-biotechnology. The distinct alignment between theoretical thermodynamic binding and experimental microbicidal assays implies that transitioning traditional coordination complexes into discrete nanoscale dimensions serves as an effective strategy to maximize surface-to-volume interactions and enhance cellular membrane permeability. These results highlight the chemical feasibility of utilizing transition metal architectures as potent platforms to combat persistent bacterial phenotypes, opening alternative pathways for developing structural frameworks in material sciences aimed at biological mitigation.

7.2. Limitations

While the synthesized nanomaterials demonstrated exceptional preliminary antibacterial profiles in vitro, several critical limitations must be recognized to maintain scientific objectivity. First, the evaluation of the specific enzymatic inhibition mechanisms (such as DNA gyrase suppression) remains strictly theoretical, based on in silico molecular docking models, lacking direct cell-free enzymatic assay verification. Second, all biological screening parameters were established exclusively through in vitro methodologies. Consequently, the in vivo pharmacological efficacy, metabolic stability, tissue distribution, and systemic bioavailability profiles of these metal–organic systems remain entirely unexplored. Most importantly, the systemic safety margin and biocompatibility of these platforms have not yet been validated due to the absence of comprehensive cytotoxicity evaluations against human cell lines or standard animal toxicity screenings.

7.3. Future Research Directions

To address the aforementioned limitations and advance the scientific maturity of these coordinated architectures, future investigations should focus on the following milestones:

1. Execute rigorous in vitro cytotoxicity assays (e.g., MTT assays) using normal human cell lines to establish clear therapeutic indices and cellular safety margins.

2. Conduct quantitative cell-free enzyme inhibition assays against isolated bacterial DNA gyrase and FabH proteins to experimentally validate the computational docking predictions.

3. Advance the most promising frameworks (specifically the nano-sized Cu(II), Ag(I) complexes into appropriate animal models to assess their real-world antimicrobial dynamics, metabolic paths, and potential systemic toxicity.

Authors' Contributions Statement

A.M.K. carried out the synthesis of the Schiff base ligand and its metal complexes, performed physical and spectral measurements, and drafted the manuscript. WIY participated in the research design, supervised the chemical and biological experiments, analyzed the molecular docking studies, and critically revised the final manuscript. All authors have read and agreed to the published version of the manuscript.

Acknowledgements

The authors thank the University of Kufa for the research opportunities. The authors would like to acknowledge the use of the Gemini large language model (developed by Google) solely for grammatical refinement, language polishing, and reference formatting assistance during the preparation of this manuscript. The AI tool was not involved in data generation, scientific interpretation, or core conceptual conclusions, and the authors hold full accountability for the integrity of the final content.

References

1. Arulmurugan, S., Kavitha, H. P., & Venkatraman, B. (2010). Biological activities of Schiff base and its complexes: a review. Rasayan Journal of Chemistry, 3(3), 385–410.
2. Da Silva, C. M., da Silva, D. L., Modolo, L. V., Alves, R. B., de Resende, M. A., Martins, C. V., & de Fátima, A. (2011). Schiff bases: A short review of their antimicrobial activities. Journal of Advanced Research, 2(1), 1–8.
3. Mushtaq, I., et al. (2024). Pharmaceutical significance of Schiff bases: an overview. Future Journal of Pharmaceutical Sciences, 10(1), 16.
4. Th, M. N., Pushpavathi, I., Vishwanath, R. S., Ke, K. S., Upendranath, K., & Ashoka, G. B. (2024). Synthesis of new electrochemically activated sulfadiazine azo dyes and its theoretical studies with LFPs, antioxidant application. Materials Science and Engineering: B, 305, 117400.
5. Yadav, M., et al. (2023). Pharmaceutical properties of macrocyclic Schiff base transition metal complexes: urgent need in today's world. Inorganica Chimica Acta, 546, 121300.
6. El-Sonbati, A. A., El-Bindary, A. A., Mansour, N. M., & El-Zahed, M. M. (2025). Novel bivalent transition metal complexes based on a 2-amino-3-hydroxypyridine Schiff base ligand: synthesis elucidation, antimicrobial evaluation, antioxidant and molecular docking studies. BMC Chemistry, 19, 177.
7. Lestari, P.D., N. Farida, and I.W. Dasna(2025). Synthesis, Structure, Hirshfeld Surface Analysis, and Antibacterial Activity of [Ni (3-NH_2py) $_4Cl_2$] Complex (3-NH_2py= 3-aminopyridine). Jurnal Kimia Sains dan Aplikasi. 28(3): p. 106-114. DOI: https://doi.org/10.14710/jksa.28.3.106-114
8. Mahmoud, E. G., Ismail, E. H., Abdel Aziz, A. A., Abdel-Latif, S. A., & Mobarez, S. N. (2026). Synthesis, spectroscopic, characterization, antimicrobial, DNA interaction, DFT and molecular docking studies of a new Cu(II)-Schiff base complex. Scientific Reports, 16(1), 13636.
9. El-Mogazy, M. A., El-Sonbati, A. A., Diab, M. A., El-Zahed, M. M., Salama, H. M., & Negm, E., et al. (2024). Synthesis, spectroscopic, thermal, DNA binding, antibacterial, antifungal, and molecular docking studies: antipyrine hydrazone ligand and its transition metal complexes. Journal of Molecular Liquids, 409, 125543.
10. Issam A.M., Huda Salah Kareem, Muhsin Jaber Jweeg, M.N. Mohammed, Thamer Adnan Abdullah, Oday I. Abdullah, Chiya Othman Hassan. Pol. J. Chem. Tech., Vol. 26, No. 4, 2024, Polish Journal of Chemical Technology, 26, 4, 104—113, 10.2478/pjct-2024-0046. Development, Comprehensive Characterization, and Antimicrobial Activity Evaluation of a Novel Class of Symmetrical 1,3-Benzoxazine Derivatives

11. Yahiya, Y. I., Yahya, W. I., Witwit, I. N., & Ali, A. A. M. (2023). Synthesis, Identification, and Biological Activity as Antibacterial of Transitional Bivalent Metal Complexes Derived from A new (azo-Schiff) Base Ligand. Latin American Journal of Pharmacy, 42, 224–228.
12. Desai, K., Shah, A., Bhanusali, A., Lad, H., Saraiya, R., Agrawal, S., Patel, K., Patel, A., Sachapara, B., Suthar, A., Champaneriya, M., Joshi, K., Kadam, Y. K., Patel, R., Dholakiya, B., Malek, N., Patel, V., & Shah, A. (2025). Exploring the antibacterial activity of novel Schiff bases: A comprehensive In vitro and In silico analysis. Total Chemistry, 1, Article 100004. https://doi.org/10.1016/j.totche.2025.100004.
13. Exploring the antibacterial activity of novel Monika, Arpna, Pallavi Bhardwaj . Schiff Base Metal Chloride Complexes of Dapsone and Pyridine-2-Carboxaldehyde Their Synthesis, Characterization, and Antifungal Properties. *Afr. J. Biomed. Res. Vol. 28(1) (January 2025); 09-13* .
14. Keshavarzian, E., et al. (2022). Heterodinuclear Cu–Gd (3d–4f) complex with di-compartmental Schiff base ligand in biological activity: Synthesis, crystal structure, catecholase activity and DNA & BSA-binding studies. Journal of Molecular Liquids, 345, 117785.
15. Mohammed, N. L., Al-Shawi, J. M. S., & Kadhim, M. J. (2018). Synthesis, Characterization and Thermal Studies of Schiff Bases Derived from 2,4-Dihydroxybenzaldehyde and their Complexes with Co(II), Ni(II), Cu(II). International Journal of Scientific Engineering and Research (IJSER), 7(1), 31–40.
16. Desalegn, T. T. (2023). Synthesis, Characterization, and Biological Activities of Schiff Bases and Their Transition Metal Complexes. World Journal of Applied Chemistry, 8(2), 22–33.
17. Gajalakshmi, B., Aswini, D., Kiruthiga, K., Kalaivani, S. R., Rajamani, K., & Anthony, R. (2024). Synthesis, Characterization, and Catalytic Applications of Schiff-Base Metal Complexes. Engineering Proceedings, 61, 26.
18. Turan, N., et al. (2022). Some metal chelates with Schiff base ligand: synthesis, structure elucidation, thermal behavior, XRD evaluation, antioxidant activity, enzyme inhibition, and molecular docking studies. Molecular Diversity, 26(5), 2459–2472.
19. Sankar, R., & Sharmila, T. M. (2023). Schiff bases-based metallo complexes and their crucial role in the realm of pharmacology: A review. Results in Chemistry, 6, 101179.
20. Martin, K., Magdaléna, D., Jiří, R., Klára, K., František, T., Jiřina, S., & Jarmila, V. (2017). Sulfadiazine Salicylaldehyde-Based Schiff Bases: Synthesis, Antimicrobial Activity, and Cytotoxicity. Molecules, 22(9), 1573.
21. Mudhi, M. A., Waheed, E. J., & Hussein, M. S. (2023). New Ligand-Based Metal Complexes: Synthesis, Spectroscopic Characterization, Thermal Behavior, Anticancer Properties, and Biological Activity. Samarra Journal of Pure and Applied Science, 5(2).
22. Ratia, C., et al. (2023). Novel gold(III)-dithiocarbamate complex targeting bacterial thioredoxin reductase: Antimicrobial activity, synergy, toxicity, and mechanistic insights. Frontiers in Microbiology, 14, 1198473.
23. Tunç, T., & Köse, Y. (2026). Synthesis, antimicrobial evaluation, and molecular docking analysis of novel Schiff bases derived from isatoic anhydride and salicylaldehyde. International Journal of Molecular Sciences, 27(2), Article 742. https://doi.org/10.3390/ijms27020742
24. Ali, O. A. M., El-Medani, S. M., Abu Serea, M. R., & Sayed, A. S. S. (2015). Unsymmetrical Schiff base (ON) ligand on complexation with some transition metal ions: Synthesis, spectral characterization, antibacterial, fluorescence and thermal studies. Spectrochimica Acta Part A: Molecular and Biomolecular Spectroscopy, 136, 651–660.
25. Stanković, M., et al. (2024). Silver(I) complexes containing antifungal azoles: significant improvement of the anti-Candida potential of the azole drug after its coordination to the silver(I) ion. Dalton Transactions, 53, 2218–2230.
26. Mutaleb, N. S., Moshref, S. A., Zayed, S., & Mahmood, A. N. (2026). Synthesis, Characterization, Antibacterial Study, and Study of Bio Properties for New Analytical Reagents. International Journal of Environmental Chemistry, 12(1).
27. Anita, P. G., & Kavita, P. (2024). Synthesis, characterization, and biological activities of novel Schiff base ligand and its Co(II) and Mn(II) complexes: Results in Chemistry. Results in Chemistry, 7, 101221.
28. Al-Hamdani, A. A. S. (2022). Synthesis, characterization, and evaluation of the biological activity of a new azo ligand and its metal complexes. *Journal of Science and Technology*, *25*(3), 45–53.
29. Nasser, S. A., & Mahdi, H. A. (2023). Synthesis, spectral, and biological studies of some metal complexes of azo dye ligand. Journal *of Chemistry and Materials Science*, *14*(1), 11.
30. Hatem, Z. M., Abdulabbas, S. S., Abd-Alzahra, M. R., Al-Mayali, H. H., & Kareem, I. K. (2022). Synthesis and characterization of novel metal complexes with a new azo-Schiff base ligand derived from isatin and toxicological studies of its complexes as antibacterial. *International Journal of Health Sciences*, *6*(S5), 2929–2945.